Available online at www.sciencedirect.com
ScienceDirect
Journal of Hazardous Materials 155 (2008) 183–192
Journal of Hazardous Materials
www.elsevier.com/locate/jhazmat

Prediction for vented explosions in chambers with multiple obstacles

Dal Jae Park [a,*], Young Soon Lee [b], Anthony Roland Green [a]

[a] School of Safety Science, Faculty of Science, The University of New South Wales, NSW 2052, Australia
[b] Department of Safety Engineering, Faculty of Engineering, Seoul National University of Technology, Seoul 139-743, Republic of Korea

Received 1 June 2007; received in revised form 14 November 2007; accepted 15 November 2007
Available online 22 November 2007

Abstract

The predictive ability between existing models on explosion venting, such as the NFPA, Molkov and Yao equations, was examined against experimental data of peak pressures obtained in various chambers with internal obstacles. The NFPA equation yielded the highest overpressures in most cases. The Molkov and Yao equations obtained much better agreement with experiments. However, the statistical diagnosis of the data showed an underprediction of the pressures. This is undesirable for designing calculations where some margin of safety is preferable. A new empirical model derived for characterising chambers with internal obstacles correlated well with the data. In addition the new equation was further validated against a dataset published from the literature and also gave a good correlation.

Keywords: Explosion venting; Obstacle types; Vent to volume ratio; Pressure

1. Introduction

Confined or partially confined gas explosions are one of the major accidents that occur in chemical plants and buildings. In order to mitigate the adverse impact from the consequences of an internal explosion in such regions, explosion venting has been used. The crucial problem in venting is the appropriate design of the vent area necessary for an effective release of the material. An understanding of the physical phenomenon by which pressure is generated in vented explosions is important for safe venting design, and such knowledge gives the basis for the development of prediction models [1].

There are a number of empirical and semi-empirical methods that can be used for the sizing of explosion venting [2–8]. These are valid only within the validity ranges covered by the experiments. Most of these methods have been derived from experimental data measured in small- and medium-sized vessels, usually without internal obstacles [9]. Although there are some methods available for obstructed enclosures in the literature [6–8], most calculation methods do not deal methodically with internal obstacles and turbulence. More especially, empirical models derived from considering obstacle types do not seem to have been developed.

One of the main aims of this study is to derive an empirical correlation to evaluate the pressure peak occurring in chambers with different obstacles as a function of geometrical parameters. A proposed empirical model is based on a combination of parameters, which largely determine the development of gas explosions in obstructed environments. The discussion centers around the ability of models to predict the peak pressure from considering two volumes obtained by dividing chambers with obstacles into two sections. The predictive ability of some empirical models for the pressures of vented deflagrations is discussed against experimental data of Park et al. [10]. Also, the results calculated from the new model are compared to the experimental values of peak pressure reported in Park et al. [10]. For the regression and the fitting of the parameters of the proposed correlation, the total of 30 experimental variables were employed and approximately 150 explosion tests were performed inside five chambers. In the measurements of Park et al. [10], each variable was repeated at least five times in order to ensure reproducibility. The results were averaged and the average results were presented. Finally, the new model is validated against experimental data published by Ibrahim and Masri [11].

* Corresponding author. Tel.: +61 2 9385 5002; fax: +61 2 9385 6190.
E-mail addresses: d.park@student.unsw.edu.au, pdj70@snut.ac.kr (D.J. Park), lysoon@snut.ac.kr (Y.S. Lee), a.green@unsw.edu.au (A.R. Green).

0304-3894/$ – see front matter © 2007 Elsevier B.V. All rights reserved.
doi:10.1016/j.jhazmat.2007.11.052

Nomenclature

Nomenclature

A_v	vent area (m^2)
A_s	surface area of vessel (m^2)
A_x	cross-sectional area of vessel (m^2)
$\bar{A}$	vent area ratio
Br	Bradley number
c_o	sound speed (m/s)
C	coefficient depending on explosive mixture
C_d	discharge coefficient
E_o	expansion ratio
L_f	flame path length (m)
p	pressure (Pa)
p_a	atmospheric pressure (Pa)
S_L	laminar flame speed (m/s)
S_T	turbulent flame speed (m/s)
$\bar{S}_F$	mean flame velocity (m/s)
$\bar{S}_o$	ratio of the gas velocity ahead the flame front and the acoustic velocity in the unburnt gas
u'	root mean square of fluid velocity fluctuations (m/s)
V	volume (m^3)

Greek symbols

β	turbulence factor
μ	generalized discharge coefficient
γ	adiabatic coefficient
χ	turbulence factor, describing the flame stretch by turbulence
ρ_{uo}	unburnt gas density (kg/m^3)
ρ_{bo}	burnt gas density (kg/m^3)
π	dimensionless pressure

Subscripts

L	laminar
T	turbulent
b	burnt gas
u	unburnt gas
o	initial state
d	discharge
red	reduced (pressure)
stat	static (activation pressure)

2. Empirical correlations for overpressures in vented explosions

Bradley and Mitcheson [2,3] have presented an alternative venting parameter, $\bar{A}/\bar{S}_o$ for combustion venting for explosions in a spherical vessel with central ignition. $\bar{A}/\bar{S}_o$ is the dimensionless vent ratio of $\bar{A}$ and $\bar{S}_o$. The two dimensionless parameters are defined below:

$$\bar{A} = \frac{C_d A_v}{A_s} \tag{1}$$

$$\bar{S}_o = \frac{S_{uo}}{c_o}\left(\frac{\rho_{uo}}{\rho_{bo}} - 1\right) = \frac{S_{uo}}{c_o}(E_o - 1) \tag{2}$$

with

$$c_o = \left(\frac{\gamma_u P_o}{\rho_{uo}}\right)^{0.5} \tag{3}$$

From the numerical solutions of the two models mentioned above, Bradley and Mitcheson [2,3] have derived the following equations:

$$p_{red} = p_{stat} = 2.43\left(\frac{\bar{A}}{\bar{S}_o}\right)^{-0.6993} \quad \text{for } p_{stat} \geq 1\ \text{bar g} \tag{4}$$

$$p_{red} = p_{stat} = 12.46\left(\frac{\bar{A}}{\bar{S}_o}\right) \quad \text{for } p_{stat} \geq 1\ \text{bar g} \tag{5}$$

$$p_{red} = 4.82 p_{stat}^{0.375}\left(\frac{\bar{A}}{\bar{S}_o}\right)^{-1.25} \tag{6}$$

Eqs. (4) and (5) are valid for cases when a single pressure peak is observed in the vented vessel and Eq. (6) is valid for vented explosions where the pressure exhibits two peaks [9]. These correlations include the peak overpressure and the laminar burning velocity, whereas no effect of turbulence and initial pressure are considered.

In order to correlate p_{red} on the same dimensionless ratio $\bar{A}/\bar{S}_o$, Bradley and Mitcheson [2,3] have cited some correlations previously derived, such as Eq. (7) of Cubbage and Simmonds [12] and Eq. (8) of Yao [13]. Yao [13] introduced the dependence of the flame velocity on an empirical turbulence factor, χ, which can be defined as the ratio of turbulent to laminar flame surface. For smoothly opening vents, Yao [13] suggested a value of $\chi = 3$ and for bursting diaphragms, $\chi = 4$. Bradley and Mitcheson [2,3] suggested a value for $\chi = 4$.

$$p_{red} = 0.365\left(\frac{\bar{A}}{\bar{S}_o}\right)^{-1} \tag{7}$$

$$p_{red} = \left[\frac{0.375\chi^{0.675}E_o^{7/6}}{E_o - 1}\right]^2\left(\frac{\bar{A}}{\bar{S}_o}\right)^{-2} \tag{8}$$

Further critical examinations of various existing formulas and especially, of their extrapolation within and beyond their recommended validity range, have been represented by Molkov et al. [6] and Molkov et al. [7]. Molkov et al. [7] presented "a new correlation" based on two new dimensionless numbers, Br and χ/μ, which include all important parameters of a vented deflagration. The deflagration-outflow-interaction number χ/μ was derived by fitting the calculated pressure–time curves to the experimental data. The Bradley number Br is closely related to the dimensionless number $\bar{A}/\bar{S}_o$ introduced by Bradley and Mitcheson [2,3]. Eq. (12) is valid for unobstructed enclosures [7], however, Razus and Krause [9] mentioned that it is also available for obstructed enclosures.

$$Br = \frac{A_v}{V^{2/3}}\frac{c_o}{S_{uo}(E_o - (1 - 1/\gamma_b)/(1 - 1/\gamma_u))} \tag{9}$$

$$\frac{\chi}{\mu} = 0.9\left[\frac{(1+10V^{1/3})(1+0.5Br)}{1+\pi_v}\right]^{0.37} \quad (10)$$

$$\pi_v = \frac{p_{stat}(\text{bar\_abs})}{p_o} \quad (11)$$

$$\pi_{red} = 9.8\left[\frac{Br(E_o-1)}{(36\pi_o)^{1/3}\sqrt{\gamma_u}}\frac{\mu}{\chi}\right]^{-2.4} \quad (12)$$

For the venting of low strength structures, but without restrictions due to vessel shape, and provided *L*/*D* does not exceed a value of 3, the NFPA 68 [5] recommends the following equation:

$$p_{red} = (CA_s)^2 A_v^{-2} \quad p_{stat} \le 0.1 \text{ bar g} \quad (13)$$

where C is a coefficient depending on explosive mixture, and the fuel gases are methane ($C = 0.037\ \text{bar}^{1/2}$) and propane ($C = 0.045\ \text{bar}^{1/2}$).

3. Comparison of empirical model prediction with experimental results

In order to examine the predictive ability of existing models on explosion venting, the experimental data obtained from the experiments of Park et al. [10] have been used. Five explosion chambers were employed in the experiments that were 700 mm × 700 mm in cross-section with a large top-venting area, A_v, of 700 mm × 210 mm. The chambers were designed at 200 mm height intervals, and the maximum height of the chambers was 1000 mm. Each chamber was employed to examine the flame interaction with three different multiple obstacles: cylindrical, square and triangular bars with blockage ratios of 30 and 42.85%. The methane concentration in air was 10% in each chamber.

The experimental data illustrates the effect of volume ratio obtained by varying the chamber volume with a constant vent area. As the vent to volume ratio decreased, the observed internal pressure peak increased, regardless of obstacle types. With the $A_v/V^{2/3}$ ratio in the range of 0.69–0.44, only one peak pressure was observed on the pressure curve. However, with ratios of less than 0.33, two peak pressures were observed. Across the ratio range of 0.69–0.24, the first peak pressure was found to be insensitive to the obstacle geometries and the obstruction ratios.

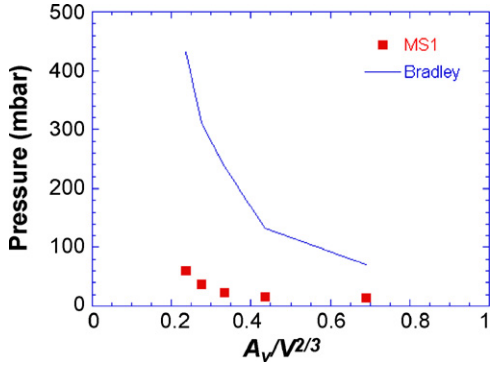

Fig. 1. Calculated pressures by Bradley model versus vent to volume ratios for multiple square bars of 0.3 BR.

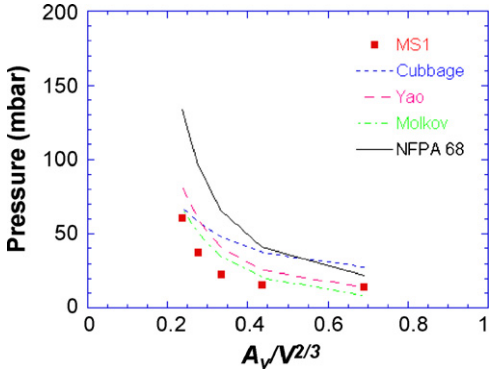

Fig. 2. Calculated pressures by NFPA, Cubbage, Yao and Molkov models versus vent to volume ratios for multiple square bars of 0.3 BR.

However, as the ratio decreased from 0.33 to 0.24, a second peak pressure became sensitive to both the obstacle geometries and the obstruction ratios. The triangular obstacle resulted in the highest pressure while the lowest one was obtained with the cylinder bars, and the higher obstruction caused the higher overpressure.

The five empirical relationships discussed in this work have been compared with the experimental data that used square bars in the different explosion chambers. The models were those of Bradley (Eq. (5)), Cubbage (Eq. (7)), Yao (Eq. (8)), Molkov (Eq. (12)) and from NFPA 68 (Eq. (13)). The calculated maximum overpressure is plotted against the dimensionless parameter, $A_v/V^{2/3}$ and is shown in Figs. 1 and 2, where data are presented

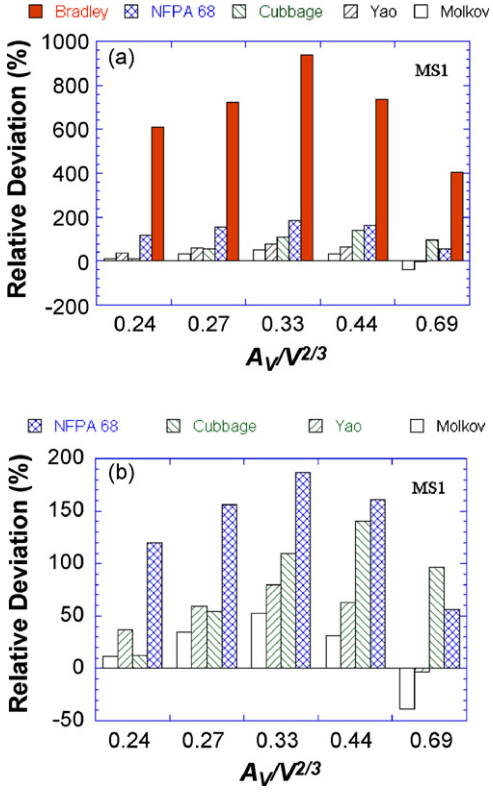

Fig. 3. Relative deviations between the calculated and the measured overpressures at different volume ratios for square bars of 0.3 BR: (a) five models and (b) four models.

Table 1
Relative errors (%) between predictions and measurements for overpressures

$A_v/V^{2/3}$	MS1				MS2			
	CM	YM	MM	NM	CM	YM	MM	NM
0.24	12.46	37.03	11.80	119.82	−18.38	−0.55	−18.86	59.52
0.27	54.11	59.68	35.27	155.96	21.47	25.86	6.62	101.75
0.33	109.26	79.55	52.90	187.46	36.97	17.52	0.08	88.16
0.44	140.15	62.64	31.51	161.12	186.36	93.93	56.81	211.36
0.70	96.45	−2.83	−39	56.73	163.55	30.35	−18.17	110.27
$A_v/V^{2/3}$	MT1				MT2			
	CM	YM	MM	NM	CM	YM	MM	NM
0.24	−4.8	15.99	−5.36	86.06	−32.9	−18.24	−33.29	31.14
0.27	35.77	40.68	19.18	125.52	10.01	13.99	−3.42	82.73
0.33	67.19	43.45	22.16	129.66	11.75	−4.10	−18.33	53.52
0.44	108.03	40.89	13.92	126.19	160.33	76.30	42.56	183.05
0.70	80.80	−10.57	−43.86	44.25	149.54	23.42	−22.52	99.09
$A_v/V^{2/3}$	MC1				MC2			
	CM	YM	MM	NM	CM	YM	MM	NM
0.24	64.45	100.38	63.49	221.43	18.19	44.02	17.50	131.02
0.27	75.79	82.14	54.31	191.98	50.12	55.55	31.78	149.35
0.33	133.20	100.09	70.39	220.35	98.59	70.39	45.10	172.80
0.44	122.61	50.76	21.9	142.04	182.51	91.33	54.70	207.17
0.70	75.87	−13.01	−45.39	40.31	119.31	8.47	−31.90	74.98

CM (Cubbage model); YM (Yao model); MM (Molkov model); NM (NFPA 68 model).

for a blockage ratio of 0.3 from the five chambers with a constant venting area of 700 mm × 210 mm. It can clearly be seen that the Bradley model overpredicted the overpressure compared to both the experimental results and the other models.

The relative deviations between the predictions and the measurements is calculated as 100 $(P_{cal}-P_{exp})/P_{exp}$, and the results applied to chambers for square bars of 0.3 BR are displayed in Fig. 3. This figure clearly indicates the failure of Bradley model with the error being large and above 400%. This model seems to be overly conservative and will not be compared with other experimental data. Table 1 presents the relative errors (%) between the measured and predicted overpressure for each obstacle.

Figs. 4 and 5 present a comparison between predictions and measurements for overpressure for the different multiple bars at 0.3 and 0.43 BR, respectively. The experimental data illustrates the effect of volume ratio obtained by varying the chamber volume with a constant vent area. Increasing the chamber volume, i.e., decreasing the vent to volume ratio was found to increase the observed internal pressure peak, regardless of obstacle types.

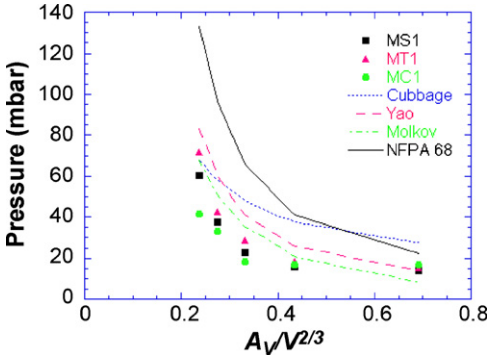

Fig. 4. Comparison between experiments and predictions for overpressure versus vent to volume ratios for different multiple bars of 0.3 BR.

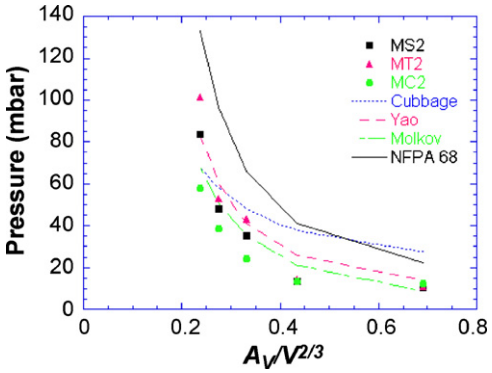

Fig. 5. Comparison between experiments and predictions for overpressure versus vent to volume ratios for different multiple bars of 0.43 BR.

As shown in Figs. 4 and 5, as a general trend, the highest predictions of the reduced pressures are given by the NFPA model, regardless of both obstacle types and obstacle obstructions. For square bars with 0.3 BR as shown in Fig. 4, the Cubbage model overpredicts the peak pressures at all values of vent to volume ratios.

As the vent to volume ratio increased, the relative error shown by the Cubbage model predictions were generally increasing. The smallest error occurred at a vent ratio of 0.24 where the relative error was about 12%. Both the Yao and Molkov models in the vent ratio range of 0.24–0.44 overpredicted the pressures, but underpredicted the pressure at vent ratio of 0.7 regardless of obstacle geometries. In case of triangular bars, the Cubbage model underpredicted the pressures at a vent ratio of 0.24. While it was in good agreement for a blockage ratio of 0.3 (<5% error), the agreement was worse at the higher blockage ratio. As shown in Fig. 5, for larger square and triangular bars (0.43 BR), the Cubbage, Yao and Molkov models underpredicted the pressures at vent ratios of 0.24 but overpredicted them at other vent ratios, The exception was the Molkov model at a vent ratio of 0.7 for all obstacles.

To determine the degree of agreement between predictions and experiments statistics diagnostics reported by Sæter [14] are applied, the values given in Table 2 are obtained. All models show on average an underprediction. NFPA model shows

Table 2
Statistical values for 4 models based on 30 experimental cases

Models	μ	$\lvert RE_{max}\rvert$	σ	$\mu \pm 2\sigma$
CM	0.35	0.65	0.27	+0.89 and, −0.19
YM	0.23	0.50	0.20	+0.65 and, −0.17
MM	0.008	0.41	0.35	+0.72 and, −0.71
NM	0.52	0.68	0.12	+0.78 and, +0.28

μ, mean of the relative error; $RE_i = (Y_i - X_i/Y_i)$, relative error; X_i, observed maximum pressure; Y_i, maximum predicted pressure; $\lvert RE_{max}\rvert$, maximum of the relative error; σ, standard deviation of the relative error.

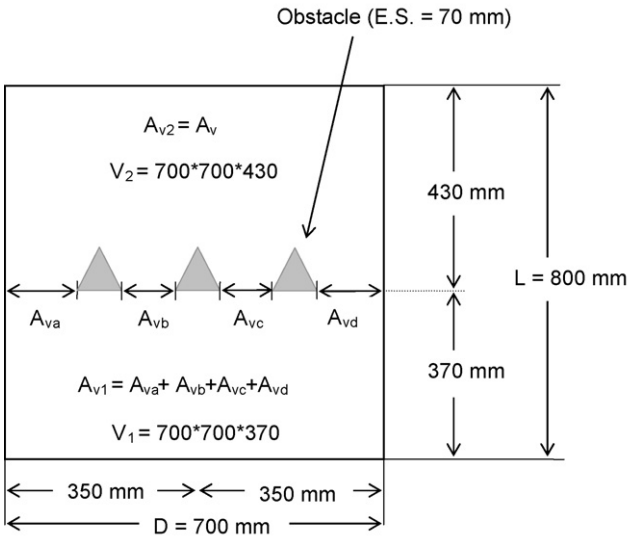

Fig. 6. An example of chamber *E* as two volumes reproduced in the prediction. $A_{v1} = 0.343\ m^2$; A_{v2} (=A_v) = $0.147\ m^2$; $V_1 = 0.1813\ m^3$; $V_2 = 0.2107\ m^3$.

on average an underprediction of 52% and the predictions indicate that there is a 95% confidence that the mean maximum overpressure will be in within +78 and +28% of the predicted value. It is found that Molkov model shows an average under prediction of only 0.8% and a 95% confidence interval of +72 and −71%.

Most of calculation correlations so far discussed deal only lightly with the boundary conditions of the expansion flow field. The boundary conditions may consist of a combination of confinement and obstacles, resulting in a shear flow and increased turbulence. Before a propagating flame encounter these conditions, it normally proceeds as laminar flame. However, as the flame interacts with the conditions, it is greatly accelerated in the wake of obstacles. The mass pushed before the interaction between flame and obstacles accumulates behind the obstacles, thus increasing pressure in a chamber. Thus, a correlation can be derived by considering the characteristics of shear layer conditions. A description of a new correlation will be given in a following section.

4. Derivation of a correlation for vented explosions

4.1. Modification of the empirical correlations

The pressure–time histories obtained from experiments of Park et al. [10] are characterised by the existence of one or two peaks. The first peak pressure (P_1) was produced by the burning of the upstream mixture located between the ignition and the obstacle. Once the pressure inside the chamber exceeds the first peak pressure, the plastic diaphragm covered in the chamber vent begins to move away from the vent, allowing unburnt mixture to escape from the chamber. The pressure within the chamber after venting starts to decrease. As the propagating flame continues to expand its surface area increases through the interaction with obstacles, and the internal pressures increases again to reach the second peak. The second peak pressure (P_2) is produced by the turbulent combustion of the trapped mixture behind the obstacle.

In order to evaluate the peak pressure, the volume below the obstacles can conceptually be considered as a vented volume into a second volume between the obstacles and the explosion chamber vent. The vent area of the first volume is the minimum area between obstacles and between obstacles and the wall of the explosion chamber and is associated with the first pressure peak (P_1). The second volume is then from this vent point to the chamber exit vent and is associated with the development of the second peak (P_2).

Fig. 6 shows one example of a sketch of the divided chamber as two volumes for the chamber *E* used in the experiments. The volume of the first section (V_1), in case of chamber with square and triangular obstacles, V_1 is calculated from the bottom of the chamber to the lower face of the obstacle, but for the circular obstacle, it is until the full diameter is reached. The volume of the secondary section (V_2) is from the lower face for the square and triangular obstacles and from the full diameter for the circular obstacle to the chamber exit. The vent area, A_{v1}, in V_1 is the cross-sectional area less the cross-sectional areas of multiple obstacles. A vent area, A_{v2}, in V_2 consists of the external vent area from the chamber (A_v used in the measurements).

In order to derive an empirical correlation to evaluate the peak pressure occurring in the chambers as a function of obstacle geometries, the evaluation of the explosion consequences

Table 3
Formulae for modified empirical models applied to the chambers divided as two volumes

Models	Equations in volume 1	Equations in volume 2	
CM	$\bar{A}_1 = \frac{C_d A_{v1}}{A_{s1}}, \quad p_{red1} = \left(\frac{\bar{A}_1}{\bar{S}_o}\right)^{-1}$	$\bar{A}_2 = \frac{C_d A_{v2}}{A_{s2}}, \quad p_{red2} = \left(\frac{\bar{A}_2}{\bar{S}_o}\right)^{-1}\left[\frac{(p_{red1}+p_a)}{p_a}\right]$	(14)
YM	$p_{red1} = \left[\frac{\chi^{0.675}E_o^{7/6}}{E_o-1}\right]^2\left(\frac{\bar{A}_1}{\bar{S}_o}\right)^{-2}$	$p_{red2} = \left[\frac{\chi^{0.675}E_o^{7/6}}{E_o-1}\right]^2\left(\frac{\bar{A}_2}{\bar{S}_o}\right)^{-2}\left[\frac{(p_{red1}+p_a)}{p_a}\right]$	(15)
MM	$Br_1 = \frac{A_{v1}}{V_1^{2/3}}\frac{c_o}{S_{uo}(E_o-(1-(1/\gamma_b))(1-(1/\gamma_u)))}$, $\frac{\chi}{\mu} = 0.9\left[\frac{(1+10V_1^{1/3})(1+0.5Br)}{1+\pi_v}\right]^{0.37}$, $\pi_{red1} = \left[\frac{Br_1(E_o-1)}{(36\pi_o)^{1/3}\sqrt{\gamma_u}}\frac{\mu}{\chi}\right]^{-2.4}$	$Br_2 = \frac{A_{v2}}{V_2^{2/3}}\frac{c_o}{S_{uo}(E_o-(1-(1/\gamma_b))/(1-(1/\gamma_u)))}$, $\frac{\chi}{\mu} = 0.9\left[\frac{(1+10V_2^{1/3})(1+0.5Br)}{1+\pi_v}\right]^{0.37}$, $\pi_{red2} = \left[\frac{Br_2(E_o-1)}{(36\pi_o)^{1/3}\sqrt{\gamma_u}}\frac{\mu}{\chi}\right]^{-2.4}\left[\frac{(\pi_{red1}+p_a)}{p_a}\right]$	(16)

in chambers with obstacle configurations was conceptually divided into two steps. The first step consisted in evaluating the peak pressure occurring in V_1 based on empirical models and using this value in the second stage to calculate the pressure in V_2.

Table 3 shows the modified empirical models used in calculating the pressure in each volume. The NFPA model is not employed in this section because the predictions given by the correlation in the previous section were too high, compared to both the experimental results and the other models. Note the empirical coefficients used in the original models are removed. The first volume is vented to the secondary volume through an uncovered vent and the secondary volume is vented to the atmosphere. P_{red2} occurring in V_2 includes P_{red1} occurring in V_1 as a function of the initial conditions. The maximum explosion pressure is equal to P_{red2}.

4.2. The boundary conditions

Mercx et al. [15] stated that a homogeneous obstacle configuration is fully characterised by only two parameters: a volume blockage ratio (VBR) and an obstacle size (D_o). The spacing between the obstacles is measured by a combination of these two variables. The number of obstacles met by the flame propagating from the ignition point to the outer edge of the configuration is measured by the ratio of a flame path length L_f and the spacing. The number of obstacles met by the flame is known as the most significant variable for the development of overpressure. The combined parameters to characterise the boundary conditions is proposed by Mercx et al. [15], and the combination is given by:

$$P \propto \frac{\mathrm{VBR}\, L_f}{D_o}, \tag{17}$$

4.3. The length to diameter

The majority of experimental data on which vent design is based, has been obtained in compact vessels of L/D less than 3. As discussed in Park et al. [10], the interaction between a propagating flame and obstacles in chambers with different L/D ratios in the range 0.29 to $1.43 < 1.5$ influenced the development of the process of turbulent combustion in gas explosions. As the ratio increased, the flame and pressure developments increased. As the venting of an explosion is under consideration, this ratio is another parameter. In addition, it is combined with the cross-sectional area of vessel, A_x, to the length to diameter ratio.

$$P \propto A_x^{0.5} \frac{L}{D} \tag{18}$$

4.4. The turbulence factor

Abdel-Gayed and Bradley [16] have reviewed the experimental data on turbulent burning velocity and found that S_T/S_L was a function of the turbulent Reynolds number and the ratio S_L/u'. At high turbulent Reynolds number S_T/S_L was mainly a function of S_L/u'. The ratio of turbulent to laminar burning velocity (S_T/S_L) is known as the turbulence factor, β. In vent design practice the effect of turbulence induced by obstacles is allowed for by the introduction of β. Although some values for β are suggested in literature, experimentally determined values are sparse [17].

The most experimental data on the influence of obstacles showed that the obstacles produce turbulence in the unburned gases set in motion by the advancing flame, and the turbulence is formed behind the obstacle. As the propagating flame encounters this turbulence generated in the wake of obstacle, the combustion rate increases and the explosion pressure rise rate increases. In the present work, the turbulent burning velocity (S_T) is replaced by the mean flame velocity ($\bar{S}_F$) corresponding to stage IV reported in Park et al. [10]. When the mean flame velocity is unknown, it is difficult to predict the value, as it depends on the reactive mixture, on the flow and on geometry. In this case, it is suggested that maximum flame speed is used or the turbulent burning velocity is converted to a flame speed. This method is applied to the experiments of Ibrahim and Masri [11] as a validation to the equation that was derived here. The use of the maximum flame speed still gave a good correlation with the experimental overpressures and may be due to the relative importance of the regression constant, c, in Eq. (21). The turbulent flame propagation and the explosion pressure are sensitive to obstacle geometries. This is recognized by the experiments performed by Masri et al. [18], Ibrahim and Masri [11], Ibrahim et al. [19] and Hargrave et al. [20]. It is necessary to include the shape factor of obstacles to the turbulence factor.

$$P \propto C_D \frac{\bar{S}_F}{S_L} \tag{19}$$

where, C_D is a shape factor of obstacle, and the values are taken as: 1.2 for circular cylinder, 2.0 for square cylinder and 2.2 for triangular cylinder [21].

4.5. The parameter combination

If the three factors such as the boundary conditions, the length to diameter ratio and the turbulence factor are considered together based on modified correlation models, a general exponential relation can be given by:

$$p_{red} = p_{red2} C, \tag{20}$$

$$C = \exp\left[a\left(\mathrm{VBR}\frac{L_f}{D_o}\right) + b\left(A_x^{0.5}\frac{L}{D}\right) + c\left(C_D\frac{\bar{S}_F}{S_L}\right) + d\right] \tag{21}$$

5. Results and discussion

The postulated combination of parameters is evaluated for all experiments reported in Park et al. [10] and correlated with the experimentally observed explosion overpressures. Once the geometric dimensions of the divided chamber configuration are known, it is possible to calculate p_{red2}. From the approximation $p_{measured} = p_{red2} C$, C can be determined from the experimental data by calculating p_{red2}. Independently C can be calculated by the formula (21) mentioned above.

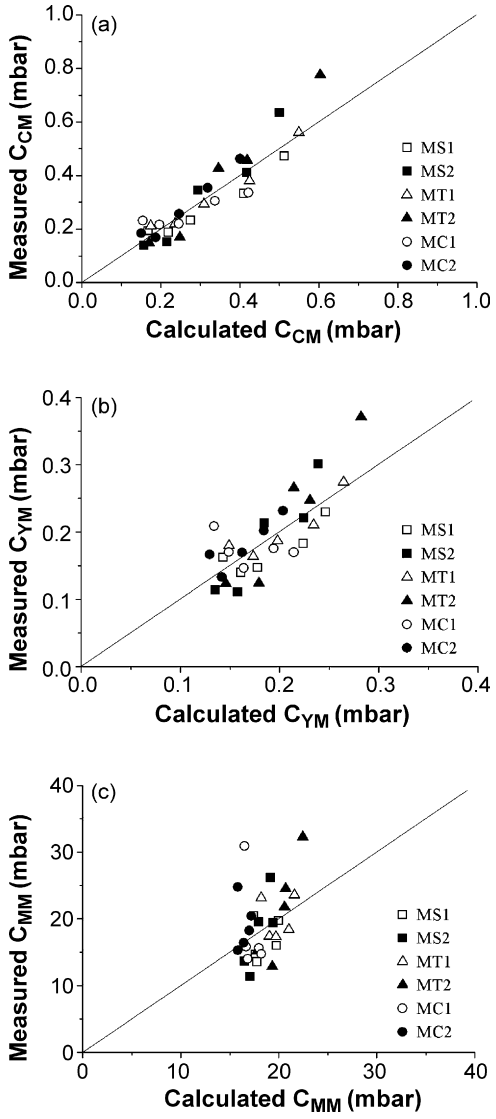

Fig. 7. Correlation dependence between the values of C obtained from the experimental data and those calculated theoretically. (a) Eq. (14), (b) Eq. (15) and (c) Eq. (16).

The correlations obtained from Eqs. (14)–(16) are graphically represented in Fig. 7. The correlation R^2 being equal to 0.84 for modified Cubbage model, 0.56 for modified Yao model and 0.13 for modified Molkov model. The regression curve obtained from the Cubbage model was the best of the three models with a standard deviation is 0.19. The obtained regression curve has the following constants: $a = -0.376$, $b = 1.046$, $c = 0.092$ and $d = -2.147$. a, b, c, and d are constants which determine the best fit correlations.

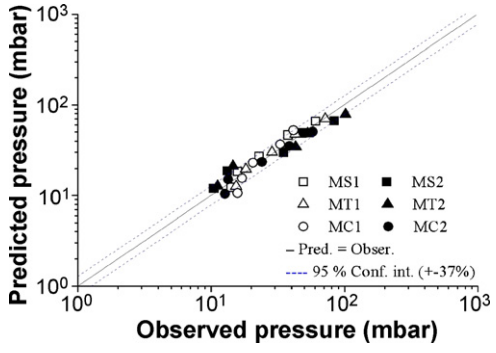

Fig. 8. Comparison of model values calculated by Eq. (22) with experimental data.

Table 4
Measured and predicted overpressures, and relative errors (RE_i)

Obstacles	$A_v/V^{2/3}$	Experiments (mbar)	Predictions (mbar)	Error (%)
MS1	0.70	14.1	12.29	−14.67
	0.44	15.74	18.38	14.40
	0.33	22.89	27.21	15.89
	0.27	37.7	46.53	18.99
	0.24	60.64	65.94	8.038
MS2	0.70	10.51	11.99	12.39
	0.44	13.2	18.72	29.49
	0.33	34.97	29.95	−16.73
	0.27	47.83	48.88	2.16
	0.24	83.56	66.37	−25.88
MT1	0.70	15.32	12.63	−21.25
	0.44	18.17	*19.58*	7.20
	0.33	28.65	30.17	5.06
	0.27	42.79	47.67	10.24
	0.24	71.64	69.81	−2.61
MT2	0.70	11.1	12.73	12.82
	0.44	14.52	21.16	31.38
	0.33	42.86	34.69	−23.53
	0.27	52.81	48.31	−9.29
	0.24	101.64	78.66	−29.21
MC1	0.70	15.75	10.60	−48.56
	0.44	16.98	15.57	−9.04
	0.33	20.54	23.08	11.02
	0.27	33.05	36.72	10.00
	0.24	41.47	52.41	20.88
MC2	0.70	12.63	10.41	−21.29
	0.44	13.38	15.04	11.083
	0.33	24.12	23.47	−2.73
	0.27	38.7	35.28	−9.68
	0.24	57.7	50.46	−14.34

Combining Eqs. (14), (20) and (21) gives the following formula:

$$p_{red} = \left(\frac{\bar{A}_2}{\bar{S}_o}\right)^{-1} \left[\frac{(p_{red1} + p_a)}{p_a}\right] C, \quad (22)$$

Eq. (22) allows the evaluation of the peak pressure in the divided two-chamber configurations as a function of obstacle geometries. In order to check the ability of the model proposed here the Eq. (22) was applied to the entire set of available experimental data.

Table 4 contains the relevant information for the plot. The values are plotted in a log coordinate system containing and two lines parallel to it. The diagonal corresponds to a perfect agreement between prediction and experiment. A statistical analysis shows that the mean relative error is −0.9% and the standard deviation of the relative error is 18.9%. This means that the new model shows in average an overprediction of 0.9%. A 95% confidence interval for a normal distribution is known to be within twice the standard deviation to each side of the mean. There-

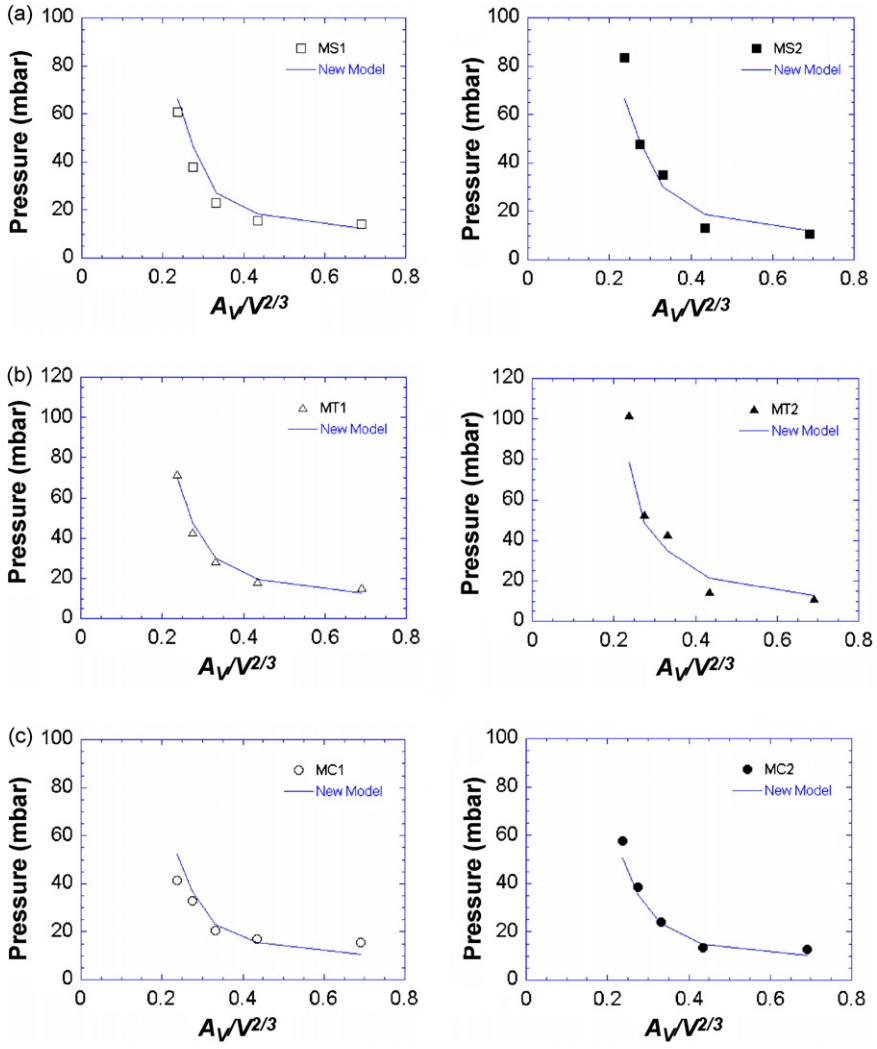

Fig. 9. Comparison of new model with experimental data obtained from chambers with square obstacles: (a) MS1 and (b) MS2, (b) MT1 and MT2, and (c) MC1 and MC2.

fore, it can be concluded that the predicted overpressure with 95% certainty will be within ±37% of the experimental values. The 95% confidence limits are indicated by dashed lines in Fig. 8.

In Fig. 8, the maximum predicted overpressure by the new model is plotted against the maximum of the experimentally observed overpressure for 30 cases. It is remarkable that such a model gives such a reasonable fit with experiment. The correlation factor is $R^2 = 0.92$, which is quite satisfactory.

The proposed empirical model is applied to verify its ability in predicting the peak pressure occurring in each chamber with each obstacle. The comparison between the results of the new model and the individual experimental data as a function of obstacle are shown in Fig. 9. Overall, comparison between measurements and predictions demonstrates that the new model provides a good simulation of overpressure within the chambers. However, the model underpredicted the pressures at about 0.24 ratio for obstacles of 0.43 BR. This may in part to due to the use of mean flame velocity observed within chamber *E* with larger obstacles. As the leading flame front interacts with the multiple obstacles until the flame reconnection behind the central obstacle, it accelerates rapidly through the constriction between the central obstacle and side obstacles, and the flame front near faces of side obstacles continues to develop in a concaved nature, this causes slower flame development at the regions. As the blockage ratio increases, the effect of the concaved nature was found to become larger.

In order to further validate the model, the prediction was compared with the results obtained by Ibrahim and Masri [11]. The enclosure was filled with a propane–air stoichiometric mixture. The dimensions of the enclosure were 195 mm × 195 mm × 545 mm. A sketch of the enclosure with a cylindrical obstruction is shown in Fig. 10. Various obstacle shapes were used: circle, square, diamond, flat plate and triangle of different sizes. Table 5 shows the various obstruction geometries that were investigated. Here, the circular obstacles are named with a *C* and a number. Squares are named in the same way with an *S*, triangles by *T*. The diamonds and flat plates are not included in the table since these cases were not predicted.

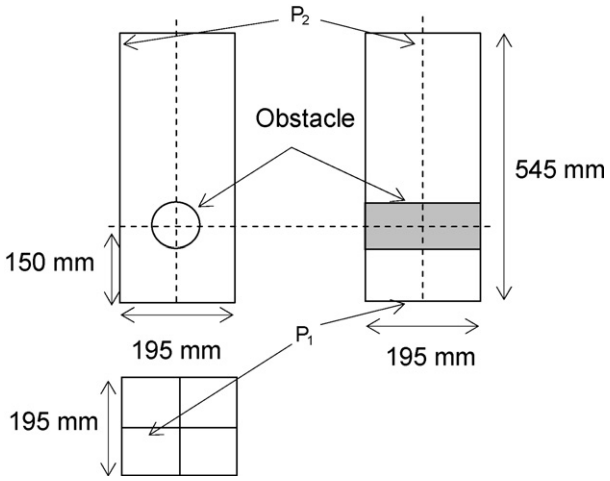

Fig. 10. Layout of the enclosure with a cylindrical obstruction.

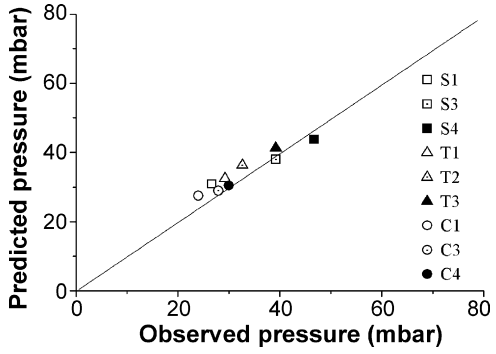

Fig. 11. Results predicted by new model with experimental data of Ibrahim and Masri [11].

For stoichiometric propane–air mixture, some constants reported by Razus and Krause [9] were used: $E_0 = 7.9$, $S_{u0} = 0.46$ m/s and $C_0 = 359$ m/s. The flame speeds by obstacles were taken from the experiments of Masri et al. [18]. In Fig. 11, the maximum predicted overpressure is plotted against the maximum of the experimentally observed overpressure for each of the 9 cases of Ibrahim and Masri [11]. Table 6 contains the relevant data for statistical analysis. When the statistical diagnostics were applied, the mean relative error was 5.22% and the standard deviation of the relative error was 7.1%. This means that the new model represents in average an underprediction of 5.22%. The agreement between the experimental data and the new model was found to be quite good. The correlation factor is $R^2 = 0.92$.

Table 5
The various obstructions [11]

Obstacle	Dimension (mm)	B.R. (%)
S1	17.0 × 17.0	8.7
S3	79.3 × 79.3	40.7
S4	108.0 × 108.0	55.4
T1	Equal sizes 24.5	12.6
T2	Equal sizes 62.0	31.8
T3	Equal sizes 103.0	52.8
C1	Diameter 19.0	9.7
C3	Diameter 106.7	54.7
C4	Diameter 139.6	71.5

Table 6
Comparison of predicted overpressures with experimental data taken from Ibrahim and Masri [11] for stoichiometric propane–air mixtures, and the relative errors (RE_i)

Obstacles	Experiments (mbar)	Predictions (mbar)	Error (%)
S1	26.6	30.86	13.82
S3	39.2	37.98	−3.20
S4	46.7	43.77	−6.68
T1	29.2	32.53	10.23
T2	32.6	36.32	10.24
T3	39.2	41.25	4.99
C1	24	27.49	12.69
C3	27.9	28.92	3.53
C4	30	30.41	1.36

6. Conclusions

The existing correlation equations were compared with the experimental data. A new empirical equation was derived, allowing the calculation of the peak pressure for vented chambers as a function of obstacle geometry. The results obtained from the new equation were compared to the experimental values of peak pressure and were validated with the available experimental data published in the literature. Summarised findings are given:

- The correlations for explosion venting were applied to verify their ability in predicting the overpressure occurring in chambers with obstacles. In most cases, examined here, the model proposed by NFPA gave the highest overpressures for a given vent to volume ratio. The correlations of Molkov and Yao gave relatively close predictions to the experimental results. However, these correlations under predicted pressure or over-predicted pressure for given geometries.
- A new empirical model to evaluate the overpressures occurring in chambers with obstacles was developed as a two-stage method. The first stage divided the chamber in two at the obstacles, and the existing correlations were applied to both chamber sections. The second stage was to apply a correction based on a combination of geometrical parameters that characterised the major determining factors for the explosion overpressure such as the boundary conditions, the length to diameter ratio and the turbulence factor. The new model, correlated well with experimental data compared to the other models tested. A good correlation of the explosion overpressure with the new model is also observed within the experimental data of Ibrahim and Masri [11].

The experimental data used here for validating the suggested correlation are obtained on a laboratory scale. Although experimental results were published in the literature by some researchers using larger scale vessels with obstructions ratios, at present, no detailed data has been used to check the correlation. Therefore, a potential scaling-up problem exists in the correlation and this could be overcome by comparing the presented correlation against larger scale experimental measurements.

References

[1] M.G. Cooper, M. Fairweather, J.P. Tite, On the mechanisms of pressure generation in vented explosions, Combust. Flame 65 (1986) 1–14.

[2] D. Bradley, A. Mitcheson, The venting of gaseous explosions in spherical vessel I—theory, Combust. Flame 32 (1978) 221–236.

[3] D. Bradley, A. Mitcheson, The venting of gaseous explosions in spherical vessel II—theory and experiment, Combust. Flame 32 (1978) 237–255.

[4] G A. Lunn, Venting of gas and dust explosions: a review of methods for calculating venting requirements for industrial containers and buildings, Health & Safety Executive Internal Report IR/L/DE/83/4, UK, 1983.

[5] NFPA 98, Guide for Venting of Deflagrations, National Fire Protection Association, Quincy, MA, USA, 1998.

[6] V. Molkov, R. Dobashi, M. Suzuki, T. Hirano, Modeling of vented hydrogen-air deflagrations and correlations for vent sizing, J. Loss Prevent. Process Ind. 12 (1999) 147–156.

[7] V. Molkov, R. Dobashi, M. Suzuki, T. Hirano, Venting of deflagrations: hydrocarbon-air and hydrogen-air systems, J. Loss Prevent. Process Ind. 13 (2000) 397–409.

[8] H. Phylaktou, Y. Liu, G.E. Andrews, Turbulence explosions: a study of the influence of the obstacle scale, in: CHISA 2000, 14th International Congress of Chemical, 1994, pp. 269–284.

[9] D.M. Razus, U. Krause, Comparison of empirical and semi-empirical calculation methods for venting of gas explosions, Fire Saf. J. 36 (2001) 1–23.

[10] D.J. Park, Y.S. Lee, A.R. Green, Experiments on the effects of multiple obstacles in vented explosion chambers, J. Hazard. Mater. 153 (2008) 340–350.

[11] S.S. Ibrahim, A.R. Masri, The effects of obstructions on overpressure resulting from premixed flame deflagration, J. Loss Prevent. Process Ind. 14 (2001) 213–221.

[12] P.A. Cubbage, W.A. Simmonds, An investigation of explosion reliefs for industrial drying ovens, Trans. Inst. Gas Eng. (1955) 470–475.

[13] C. Yao, Explosion venting of low-strength equipment and structures, J. Loss Prevent. Process Ind. 8 (1974) 1–9.

[14] O. Sæter, Modelling and simulation of gas explosion in complex geometries, Ph.D. Thesis, Telemark College, Norway, 1998.

[15] W.P.M. Mercx, A.C. Van den Berg, C.J. Hayhurst, N.J. Robertson, K.C. Moran, Developments in vapour cloud explosion blast modeling, J. Hazard. Mater. 71 (2000) 301–319.

[16] R.G. Abdel-Gayed, D. Bradley, Turbulence and turbulent flame propagation, Philos. Trans. R. Soc., London A 301 (1981) 1–25.

[17] H. Phylaktou, G.E. Andrews, Gas explosions in long closed vessels, Combust. Sci. Technol. 77 (1991) 27–39.

[18] A.R. Masri, S.S. Ibrahim, N. Nehzat, A.R. Green, Experimental study of premixed flame propagation over various solid obstructions, Exp. Therm. Fluid Sci. 21 (2000) 109–116.

[19] S.S. Ibrahim, G.K. Hargrave, T.C. Williams, Experimental investigation of flame/solid interactions in turbulent premixed combustion, Exp. Therm. Fluid Sci. 24 (2001) 99–106.

[20] G.K. Hargrave, S.J. Jarvis, T.C. Williams, A study of transient flow turbulence generation during flame/wall interactions in explosions, Meas. Sci. Technol. 13 (2002) 1036–1042.

[21] V.L. Streeter, E.B. Wylie, Fluid Mechanics, eighth ed., McGraw-Hill, New York, USA, 1985.